Research in Astronomy and Astrophysics, 24:015010 (16pp), 2024 January https://doi.org/10.1088/1674-4527/ad0826

Disturbance Observer-based Pointing Control of Leighton Chajnantor Telescope

Weirui Chen[1,2] and Zheng Wang[1,2]
[1] School of Automation, Southeast University, Nanjing 210096, China; wangz@seu.edu.cn
[2] Key Laboratory of Measurement and Control of Complex Systems of Engineering, Ministry of Education, Southeast University, Nanjing 210096, China
Received 2023 September 2; revised 2023 October 18; accepted 2023 October 27; published 2023 December 13

Abstract

Leighton Chajnantor Telescope (LCT), i.e., the former Caltech Submillimeter Observatory telescope, will be refurbished at the new site in Chajnantor Plateau, Chile in 2023. The environment of LCT will change significantly after its relocation, and the telescope will be exposed to large wind disturbances directly because its enclosure will be completely open during observation. The wind disturbance is expected to be a challenge for LCT's pointing control since the existing control method cannot reject this disturbance very well. Therefore, it is very necessary to develop a new pointing control method with good capability of disturbance rejection. In this research, a disturbance observer—based composite position controller (DOB-CPC) is designed, in which an H_∞ feedback controller is employed to compress the disturbance, and a feedforward linear quadratic regulator is employed to compensate the disturbance precisely based on the estimated disturbance signal. Moreover, a controller switching policy is adopted, which applies the proportional controller to the transient process to achieve a quick response and applies the DOB-CPC to the steady state to achieve a small position error. Numerical experiments are conducted to verify the good performance of the proposed pointing controller (i.e., DOB-CPC) for rejecting the disturbance acting on LCT.

Key words: instrumentation: miscellaneous – methods: analytical – methods: numerical – telescopes

1. Introduction

The Caltech Submillimeter Observatory (CSO) telescope was decommissioned in 2015 and will be moved to its new site at Chajnantor Plateau, Chile from its old site at Maunakea, Hawaii in 2023. After the completion of the relocation, the CSO telescope will be refurbished at the new site and renamed as the Leighton Chajnantor Telescope (LCT) (Vial et al. 2020; Chen et al. 2022). However, the relocation and refurbishment of LCT will face with new challenges for its pointing control system, because it is expected to resist strong wind disturbance at the new site, which has an average wind speed of 10 m s^{-1}, a maximum instantaneous wind speed of 30 m s^{-1}, and more frequent wind speed fluctuation (ALMA 2010). In addition, LCT will work with its enclosure open completely, because LCT is required to observe a larger area of the sky at the new site to achieve the new scientific goals (Caltech et al. 2016).

To achieve a high pointing accuracy at the new site under strong wind load, LCT's pointing control system needs to realize a pointing control with high precision, i.e., to ensure the azimuth angle and the elevation angle of LCT's antenna be within a sufficiently small deviation from position of the target source in the sky. Since LCT is a submillimeter radio telescope with a 10.4 m-diameter antenna and receives the radiation with the wavelengths from 2 mm to 350 μm, a pointing error below 3″ (i.e., 0°.000 833) is required to achieve its scientific goals,[3] which requires that the root mean square (rms) of the position error of LCT's antenna must be less than 3″. However, this pointing accuracy is very difficult to achieve when LCT is working with a strong wind load. By testing the existing proportional feedback controller of LCT on its simulation model (Chen & Wang 2022), the rms of the azimuth angle error of LCT's antenna is greater than 3″ when the wind with a speed above 10 m s^{-1} is introduced. Obviously, the performance of the existing feedback controller cannot satisfy the requirement on the pointing accuracy when the telescope is fully exposed to high-speed wind. Thus, for the purpose of keeping the pointing accuracy of LCT at the new site, it is necessary to improve the position controller of LCT.

Few work has been done to employ advanced control methods to the pointing control systems of astronomical telescopes. In practice, traditional proportional-integral (PI) controller is the most popular one applied to the pointing control systems of telescopes due to its convenience for implementing (Ravensbergen 1994; Burns 1995; Gawronski 2001; Ranka et al. 2016), although it is sensitive to wind disturbance. In the past decades, to make the position controller

[3] http://cso.caltech.edu/wiki/cso/science/overview

of radio telescopes more accurate and robust under external disturbance, many scientists and engineers have paid a lot of efforts on improving its performance. On one hand, some model-free control methods are developed since they have no strict requirements on the accuracy of the model of the telescopes' pointing control systems. For example, the active disturbance rejection controller (ADRC) is designed based on the classical feedback control framework. With the help of tracking differentiator, feedback control law, and the extended state observer (ESO), the ADRC controller can resist the internal uncertainty (e.g., the nonlinearity of the system) and the external disturbance (e.g., the wind disturbance) (Qiu et al. 2014; Ranka et al. 2015; Guo et al. 2016; Feng & Guo 2017; Deng et al. 2018; Li et al. 2019). However, as the core of ADRC controller, the ESO can only estimate rough disturbance signal and is very sensitive to parameter tuning since it is not designed based on the system's model. On the other hand, since more methods are developed to identify the models of the telescopes' pointing control systems, it is feasible to employ model-based control methods for improving the robustness. The Linear-Quadratic-Gaussian (LQG) controller is a model-based optimal control method that is widely applied to many modern radio telescopes, e.g., the Deep Space Network (DSN) (Gawronski et al. 1994; Maneri & Gawronski 2000), the Green Bank Telescope (GBT) (Gawronski & Parvin 1995), the Large Millimeter Telescope (LMT) (Gawronski & Souccar 2005), the Telescope Nazionale Galileo (TNG) telescope (Schipani et al. 2020), and the 110 m QiTai radio Telescope (QTT) (Li et al. 2017). The introduction of the LQG controller effectively restrains the vibration of these radio telescopes such that the error of the position control of their pointing control systems can be reduced under wind disturbance compared to the position error under PI controllers. As the H_2 norm limits the performance of the LQG controller, the H_∞ controller is proposed by replacing the H_2 norm with the H_∞ norm to further improve the performance of the optimal controller (Gawronski 2001).

Although many model-free or model-based control methods have been applied to telescopes' pointing control systems, the effect of disturbance can hardly be eliminated since it is not accurately estimated. An H_∞ controller was designed by Chen & Wang (2022) for LCT's pointing control system to improve its robustness for resisting wind disturbance. From the simulation results, although the H_∞ controller can significantly compress the position error of LCT's antenna, it still cannot eliminate the wind disturbance precisely. Hence, in this paper, to eliminate the wind disturbance precisely, we design a disturbance observer (DOB) to realize an accurate estimation of wind disturbance, based on which we propose a new disturbance observer-based controller (DOBC) for LCT to acquire better performance of disturbance rejection.

DOBC offers a feasible method for reducing the negative influence from external disturbance and internal uncertainty by utilizing the estimated disturbance from the DOB and feed it forward to the control signal of an electromechanical system (Choi et al. 2003; Chen et al. 2016). DOBC has been applied to many real-world systems, e.g., permanent magnet synchronous motors (PMSM) (Dai et al. 2021), missile seekers (Sadhu & Ghoshal 2011), unmanned aerial vehicles (UAV) (Huang & Chen 2022; Tripathi et al. 2022), overhead cranes (Wu et al. 2020), ship-mounted tower cranes (Qian & Fang 2019), cars with an active suspension system (Pan et al. 2016), and dual-flexible manipulators with a telescopic arm (Shang et al. 2022). For generating a compensation control signal based on the estimated disturbance, most research on designing DOBC (Sadhu & Ghoshal 2011; Pan et al. 2016; Qian & Fang 2019; Wu et al. 2020; Huang & Chen 2022; Shang et al. 2022; Tripathi et al. 2022) simply assume that the control signal (i.e., the output of the controller instead of the actuator) and the disturbance signal are of the same type (e.g., both are torques or both are forces). Based on this assumption, the estimated disturbance signal (i.e., the output of the DOB) is directly utilized as a compensation control signal (by taking it negative value) and is simply combined with feedback control signal. For example, Pan et al. (2016), Qian & Fang (2019), and Wu et al. (2020) ideally consider the feedback control signal to be force, and the disturbance acting on the controlled object is also considered as force so that the estimated disturbance signal can be directly utilized as the compensation control signal. However, in realistic control systems, the output of the controller is an electric signal (e.g., voltage) rather than force or torque. The output of the controller (i.e., the control signal) is sent to the actuator and the actuator transforms the control signal to force or torque, which directly control the object. Therefore, to compensate the disturbance, the output of the DOB, which represents some physical quantity (e.g., force or torque), must be transformed to a compensation control signal that will be sent to the actuator and transformed to the physical quantity (e.g., force or torque) acted on the controlled object. Some researchers designed a compensation gain (Chen et al. 2016) or a nonlinear continuous function (Dai et al. 2021) to transform the estimated disturbance signal to a compensation control signal. In this paper, we construct an optimal tracking control model with a linear quadratic regulator to generate a precise compensation control signal that can make the actuator output proper physical quantity relatively close to the estimated disturbance signal such that the disturbance can be compensated.

The rest of this paper is organized as follows. In Section 2, the model of LCT's pointing control system is constructed with the vibration modals of the antenna, which are the first-order and the second-order vibration modals of the antenna. Section 3 presents the design of the DOBC based on the model of LCT's pointing control system. The results and analysis of the simulation are given in Section 4 to verify the performance of

the DOBC. In Section 5, we conclude this paper and give the outlook for future research.

2. Model of LCT's Pointing Control System with Structural Vibration Modals

An accurate model of LCT's pointing control system is very important to the design of the position controller. LCT's pointing control system model was constructed in our previous work (Chen & Wang 2022), which consists of the position controller, the DC motor, the reducer box, and the antenna. There are two major vibration modals of the LCT antenna, which are the low-frequency flexible modal (i.e., the first-order vibration modal of the antenna), and the main structural vibration modal of the main reflector (i.e., the second-order vibration modal of the antenna). In our previous work, the first-order vibration modal of the antenna is already considered since it is the low-frequency flexible modal resulting from the flexible connections between the DC motor and the reducer and between the reducer and the antenna when the antenna is regarded as a rigid body. Thus, the dynamic equation of the first-order vibration modal can be formulated as shown in Equation (1). For the clarity of description, in this paper, we only consider the position control in azimuth. The method developed in this paper can also be applied to the position control in elevation.

$$J_A\ddot{\theta}_1 + D_1\dot{\theta}_1 = K_{\mathrm{RDC}}T_{\mathrm{RDC}} = K_{\mathrm{RDC}}\left(\frac{1}{N}\theta_{\mathrm{DCM}} - \theta_1\right) \tag{1}$$

where J_A is the moment of inertia of the LCT antenna; D_1 is the damping of the rigid body of the LCT antenna; K_{RDC} is the stiffness of the reducer, which takes the flexible connections among the DC motor, the reducer, and the antenna into account; T_{RDC} is the output torque of the reducer; θ_{DCM} is the rotation angle of the DC motor; and θ_1 is the output azimuth angle of the rigid body of the LCT antenna. Then, Equation (1) can be reformulated as

$$J_A\ddot{\theta}_1 + D_1\dot{\theta}_1 + K_{\mathrm{RDC}}\theta_1 = \frac{K_{\mathrm{RDC}}}{N}\theta_{\mathrm{DCM}} \tag{2}$$

Applying the Laplace transform to both sides of Equation (2) yields

$$s^2J_A\theta_1 + sD_1\theta_1 + K_{\mathrm{RDC}}\theta_1 = \frac{K_{\mathrm{RDC}}}{N}\theta_{\mathrm{DCM}} \tag{3}$$

Therefore, the transfer function of the first-order modal is

$$G(s) = \frac{\theta_1}{\theta_{\mathrm{DCM}}} = \frac{K_{\mathrm{RDC}}/N}{J_As^2 + D_1s + K_{\mathrm{RDC}}} \tag{4}$$

Naturally, we can obtain the angular velocity ω_1 of the first-order modal as

$$\begin{aligned}\omega_1 &= \sqrt{\frac{K_{\mathrm{RDC}}}{J_A}}\\ &= \sqrt{\frac{6.99\times10^7\ \mathrm{N\cdot m\cdot rad^{-1}}}{160560\ \mathrm{kg\cdot m^2}}} \approx 20.8651\ \mathrm{rad\cdot s^{-1}}\end{aligned} \tag{5}$$

So, the natural frequency of the first-order modal is $f_1 \approx 3.32$ Hz, which is also verified by the modal analysis of LCT using Ansys 2022.

Although flexible connections among the DC motor, the reducer, and the antenna are considered in the first-order modal, the antenna is still assumed to be a rigid body at present although LCT's antenna in the real world is a flexible body (which may lead to the deformations of the main reflector under the wind and gravity). Therefore, to better describe the flexibility of LCT's antenna, we introduce the structural vibration modal (which is related to the vibration of the main reflector) as the second-order vibration modal of the antenna to extend the pre-established antenna's rigid body model. By analyzing the vibration modals of LCT's antenna with Ansys 2022, we find that the natural frequency of the main structural vibration modal of the antenna is 13.004 Hz. By introducing the main structural vibration modal, the extended LCT antenna model can be formulated as follows:

$$\begin{cases} J_A\ddot{\theta}_1 + D_1\dot{\theta}_1 = T_L \\ J_A\ddot{\theta}_2 + D_2\dot{\theta}_2 + K_2\theta_2 = T_L \end{cases} \tag{6}$$

$$\theta_A = \theta_1 + \theta_2 \tag{7}$$

where J_A is the moment of inertia of LCT's antenna in azimuth; D_1, D_2 are the damping of the rigid body and the main structural vibration modal respectively; K_2 is the stiffness of the main structural vibration modal; θ_1, θ_2 are the output azimuth angles of the rigid body and the main structural vibration modal respectively; θ_A is the azimuth angle of LCT's antenna (in $\mathrm{rad\cdot s^{-1}}$); and T_L is the load torque of LCT's antenna. Among these parameters, $J_A = 160560\ \mathrm{kg\cdot m^2}$, and $D_1 = \sigma_1 = 1.7827\times10^6\ \mathrm{N\cdot m\cdot(rad\cdot s^{-1})^{-1}}$ are already known (Chen & Wang 2022); and D_2, K_2 can be calculated from the following equations (Gawronski 2008):

$$D_2 = 2\zeta_2\omega_2J_A \tag{8}$$

$$K_2 = {\omega_2}^2J_A \tag{9}$$

where $\zeta_2 = 0.01$ is the damping ratio of the main structural vibration modal; and the angular velocity ω_2 of the main structural vibration modal is

$$\omega_2 = 2\pi f_2 = 2\times\pi\times13.004 = 81.7065\ \mathrm{rad\cdot s^{-1}} \tag{10}$$

where $f_2 = 13.004$ Hz is the natural frequency of the structural vibration modal (i.e., the second-order vibration modal of the antenna).

By applying Laplace transform on both sides of Equations (6) and (7), the input-output model of LCT's antenna can be obtained as below:

$$\begin{cases} \theta_1(s) = \dfrac{T_L(s)}{J_A s^2 + D_1 s} \\ \theta_2(s) = \dfrac{T_L(s)}{J_A s^2 + D_2 s + K_2} \end{cases} \tag{11}$$

By integrating the model of LCT's antenna with two major vibration modals to the pre-established LCT's pointing control system model (Chen & Wang 2022), we can obtain the extended open-loop model of the pointing control system as shown in Figure 1.

Note that $T_L = T_S$ if the wind disturbance is not introduced to the system, where T_s is the output torque of the DC motor and reducer. Assume that $x_1 = I_{\text{ARM}}$, $x_2 = \omega_{\text{DCM}}$, $x_3 = \theta_{\text{DCM}}$, $x_4 = \theta_1$, $x_5 = \omega_{A1}$, $x_6 = \theta_2$, $x_7 = \omega_{A2}$, where I_{ARM} is the armature current of the DC motor; ω_{DCM} is the rotating speed of the DC motor; ω_{A1} and ω_{A2} are the rotating speed of the rigid body of the antenna, and the rotating speed of the main structural vibration modal of the antenna respectively; θ_{DCM} is the rotation angle of the DC motor. Then the state-space model of LCT's pointing control system with extended LCT antenna model can be written as follows:

$$\begin{cases} \dot{x}_1 = \dfrac{U_{\text{ARM}}/U_{\text{COM}}}{L_{\text{DCM}}} u_c - \dfrac{R_{\text{DCM}}}{L_{\text{DCM}}} x_1 - \dfrac{C_{\text{DCM}}}{L_{\text{DCM}}} x_2 \\ \dot{x}_2 = \dfrac{1}{J_{\text{DCM}}}\left(K_{\text{DCM}} x_1 - \sigma_1 x_2 - \dfrac{1}{N} T_L\right) \\ \dot{x}_3 = x_2 \\ \dot{x}_4 = x_5 \\ \dot{x}_5 = -\dfrac{D_1}{J_A} x_5 + \dfrac{1}{J_A} T_L \\ \dot{x}_6 = x_7 \\ \dot{x}_7 = -\dfrac{K_2}{J_A} x_6 - \dfrac{D_2}{J_A} x_7 + \dfrac{1}{J_A} T_L \end{cases} \tag{12}$$

$$y = \frac{180}{\pi}(x_4 + x_6) \tag{13}$$

with

$$T_L = \frac{K_{\text{RDC}}}{N} x_3 - K_{\text{RDC}}(x_4 + x_6) \tag{14}$$

where $x_i\,(i = 1...7)$ are the system states, y is the system output (i.e., the position of the antenna in azimuth, or the azimuth angle, in degrees), u_c is the control input (i.e., the command voltage with the maximum value of U_{COM}); and the parameters of Equations (12)–(14) are listed in Table 1. Note that T_L in Equations (12) and (14) is the load torque of the reducer, and T_L/N is the load torque of the DC motor.

It should be noted that the value of K_{DCM} (i.e., the torque coefficient of the DC motor) in Table 1 is twice the value of the real single DC motor, because there are two DC motors in the azimuth channel of the real-world LCT's pointing control system for the purpose of eliminating the backlash of the gears in the speed reduction system and they are equivalent to one DC motor in this model.

From Equations (12)–(14), the state-space model of LCT's pointing control system with extended LCT antenna model can be formulated as below:

$$\begin{cases} \dot{\boldsymbol{x}}_s = A_s \boldsymbol{x}_s + B_s u_c \\ y = C_s \boldsymbol{x}_s + D_s u_c \end{cases} \tag{15}$$

where $\boldsymbol{x}_s = [x_1\ x_2\ x_3\ x_4\ x_5\ x_6\ x_7]^T$ is the state vector; A_s, B_s, C_s, D_s are the system's parameter matrices that can be formulated as follows:

$$A = \begin{bmatrix} -\frac{R_{\text{DCM}}}{L_{\text{DCM}}} & -\frac{C_{\text{DCM}}}{L_{\text{DCM}}} & 0 & 0 & 0 & 0 & 0 \\ \frac{K_{\text{DCM}}}{J_{\text{DCM}}} & -\frac{\sigma_1}{J_{\text{DCM}}} & -\frac{K_{\text{RDC}}}{J_{\text{DCM}} N^2} & \frac{K_{\text{RDC}}}{J_{\text{DCM}} N} & 0 & \frac{K_{\text{RDC}}}{J_{\text{DCM}} N} & 0 \\ 0 & 1 & 0 & 0 & 0 & 0 & 0 \\ 0 & 0 & 0 & 0 & 1 & 0 & 0 \\ 0 & 0 & \frac{K_{\text{RDC}}}{J_A N} & -\frac{K_{\text{RDC}}}{J_A} & -\frac{D_1}{J_A} & -\frac{K_{\text{RDC}}}{J_A} & 0 \\ 0 & 0 & 0 & 0 & 1 & 0 & 0 \\ 0 & 0 & \frac{K_{\text{RDC}}}{J_A N} & -\frac{K_{\text{RDC}}}{J_A} & 0 & -\frac{K_{\text{RDC}} + K_2}{J_A} & -\frac{D_2}{J_A} \end{bmatrix} \tag{16}$$

$$B = \begin{bmatrix} \dfrac{U_{\text{ARM}}/U_{COM}}{L_{\text{DCM}}} & 0 & 0 & 0 & 0 & 0 & 0 \end{bmatrix}^T \tag{17}$$

$$C = \begin{bmatrix} 0 & 0 & 0 & 180/\pi & 0 & 180/\pi & 0 \end{bmatrix}, D = 0 \tag{18}$$

3. Design of the DOB-Based Position Controller

There exist two types of disturbances in LCT's pointing control system: one is the external disturbance, i.e., the wind load, and the other is the internal disturbance, i.e., the vibration of the flexible structure of the antenna. The two types of disturbances are coupled with each other when they act simultaneously. Whereas the DOB is known for its good performance on estimating the external and internal disturbance accurately, it is expected that the negative impacts of the external and internal disturbance can be mostly rejected if a well-designed DOB-based position controller (i.e., a position controller composed of a DOB-based feedforward controller and a feedback controller) is employed in LCT's pointing control system. Hence, in this section, we focus on the design of the DOB-based controller of LCT's pointing control system. First, we design a time-domain DOB to estimate the coupled disturbance generated by both the external disturbance (i.e., the wind load) and the internal disturbance (i.e., the structural vibration modals). Second, a suitable linear-quadratic-regulator (LQR) - based feedforward controller is designed to compensate the disturbance estimated by the DOB. Finally, we design a composite DOB-based position controller by integrating the

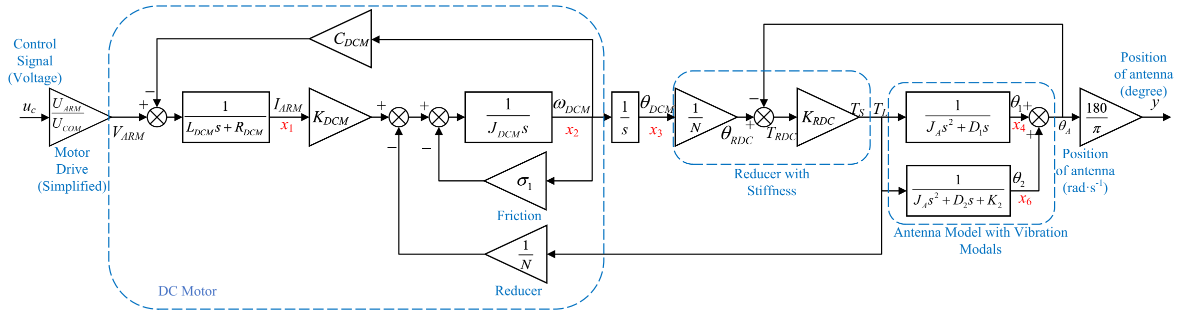

Figure 1. Diagram of the extended open-loop model of LCT's pointing control system with structural vibration modals.

Table 1
Parameters of LCT's Pointing Control System

Symbol	Definition	Value
J_A	the moment of inertia of the LCT antenna	$160560\ \mathrm{kg \cdot m^2}$
D_1	the damping of the rigid body of the LCT antenna	$1.7827 \times 10^6\ \mathrm{N \cdot m \cdot (rad \cdot s^{-1})^{-1}}$
D_2	the damping of the main structural vibration modal	$2.6237 \times 10^5\ \mathrm{N \cdot m \cdot (rad \cdot s^{-1})^{-1}}$
K_2	the stiffness of the main structural vibration modal	$1.07 \times 10^9\ \mathrm{N \cdot m \cdot rad^{-1}}$
K_{RDC}	the stiffness of the reducer	$3.498 \times 10^7\ \mathrm{N \cdot m \cdot rad^{-1}}$
L_{DCM}	the inductance of the DC motor	0.00159 H
R_{DCM}	the resistance of the DC motor	0.30 ohm
K_{DCM}	the torque coefficient of the DC motor	$0.542\ \mathrm{N \cdot m \cdot A^{-1}}$
J_{DCM}	the moment of inertia of the DC motor	$2.034 \times 10^{-3}\ \mathrm{N \cdot m \cdot s}$
C_{DCM}	the back electromotive force (EMF) coefficient of the DC motor	$0.271\ \mathrm{V \cdot (rad \cdot s^{-1})}$
σ_1	the damping coefficient of the DC motor	$4.8694 \times 10^{-5}\ \mathrm{N \cdot m \cdot (rad \cdot s^{-1})^{-1}}$
N	the reduction ratio	15 050
U_{ARM}	the armature voltage of the DC motor	115 V
U_{COM}	the maximum value of the command voltage	5 V

feedforward controller and the feedback controller (H_∞ controller or proportional controller), along with a controller switching policy for keeping good transient and steady-state performance while rejecting external and internal disturbance.

3.1. The Time Domain DOB (TD-DOB)

There exist two types of the DOB, which are the frequency domain DOB (FD-DOB) and the time domain DOB (TD-DOB) (Li et al. 2016). By taking the antenna as the controlled object (i.e., the object to be controlled by the control system) for more understandable explanations, the key idea of FD-DOB can be explained as follows: If we know the nominal model of the antenna, then we can estimate the nominal input torque signal from the inverse of the transfer function of the antenna's rigid model and the measured output azimuth angle of the antenna. In the absence of external disturbance (i.e., the wind disturbance) and the internal disturbance (i.e., the vibration of the flexible structure of the antenna), this estimated input torque signal should be consistent with the output torque signal of the motor and reducer. However, in practice, the input torque of the antenna is affected by the torque of the external disturbance (such as the wind disturbance), and the antenna's flexible modals lead to the fluctuation of the output azimuth angle, which makes the actual input torque not equal to the nominal input torque. Then, the input torque disturbances caused by internal disturbance (i.e., the vibration of the flexible structure of the antenna) and external disturbance (i.e., the wind disturbance) can be finally obtained by differentiating the actual output torque from the calculated nominal input torque. By estimating the input torque disturbances and compensating it accordingly by regulating the motor, the negative effects of the input torque disturbances on the pointing control system can be counteracted to some extent.

TD-DOB is another formulation of the DOB. Similar to FD-DOB, TD-DOB is motivated by the desire of using the model information and the input and output signals of the model to extract the disturbance signals from the input signals. Therefore, TD-DOB also requires a nominal model of the antenna, the measured output azimuth angle, and the output torque signal from the motor and reducer. However, unlike FD-DOB which directly utilizes the inverse of the transfer function of the antenna's rigid model to estimate the disturbance signal in the

frequency domain, TD-DOB is constructed in the time domain by augmenting the antenna model in the form of a state-space by introducing a disturbance term, and thus constructing an observer to estimate the augmented state including the disturbances.

Considering that the TD-DOB is convenient to implement on embedded hardware platforms, we adopt the TD-DOB for disturbance estimation. At first, to estimate the composite disturbance generated by both the external disturbance (i.e., the wind load) and the internal disturbance (i.e., the structural vibration modals), we take the rigid body model of LCT's antenna as a nominal one, which can be obtained from Equation (12) as the following state-space equations:

$$\begin{cases} \dot{\boldsymbol{x}}_a = A_n \boldsymbol{x}_a + B_n(T_L + T_d) \\ \theta_A = C_n \boldsymbol{x}_a \end{cases} \tag{19}$$

where $\boldsymbol{x}_a = [\omega_{A1} \ \ \theta_1]$ is the vector of the states of the rigid body model of the antenna; T_d is the torque generated by the wind load; and A_n, B_n, C_n are the matrices of the system parameters defined as below:

$$A_n = \begin{bmatrix} -\dfrac{D_1}{J_A} & 0 \\ 1 & 0 \end{bmatrix}, B_n = \begin{bmatrix} \dfrac{1}{J_A} \\ 0 \end{bmatrix}, C_n = [0 \ \ 1] \tag{20}$$

To facilitate the implementation of the DOB on embedded hardware platforms, inspired by Yang et al. (2017), the TD-DOB is designed as follows

$$\begin{cases} \dot{z} = -LB_n(z + \boldsymbol{L}\boldsymbol{x}_a) - L(A_n \boldsymbol{x}_a + B_n T_s) \\ \widehat{T}_d = z + \boldsymbol{L}\boldsymbol{x}_a \end{cases} \tag{21}$$

where $\widehat{T}_d$ is the estimated torque of the internal and external disturbance; $L > 0$ is the gain matrix of the TD-DOB, which needs to be further designed; z is the auxiliary variable of the DOB; and T_s is the nominal load torque of LCT's antenna without any disturbances. It should be noted that T_s can hardly be measured directly and hence it must be calculated according to the position of the antenna $\theta_A = \theta_1 + \theta_2$ and the speed of the motor ω_{DCM} as follows:

$$T_s(t) = K_{\mathrm{RDC}}\left(\frac{1}{N}\int_0^t \omega_{\mathrm{DCM}}(\tau)d\tau - \theta_A(t)\right) \tag{22}$$

Moreover, a first-order low-pass filter is designed to provide the proper estimated disturbance signal for designing a realizable feedforward controller, which is given by

$$P(s) = \frac{1}{\lambda s + 1} \tag{23}$$

where $\lambda \in \mathbb{R}^+$ is the parameter of the first-order low-pass filter. Therefore, the ultimate output signal $\widehat{T}_{do}$ of the TD-DOB is

$$\widehat{T}_{do} = P(s)\widehat{T}_d = \frac{\widehat{T}_d}{\lambda s + 1} \tag{24}$$

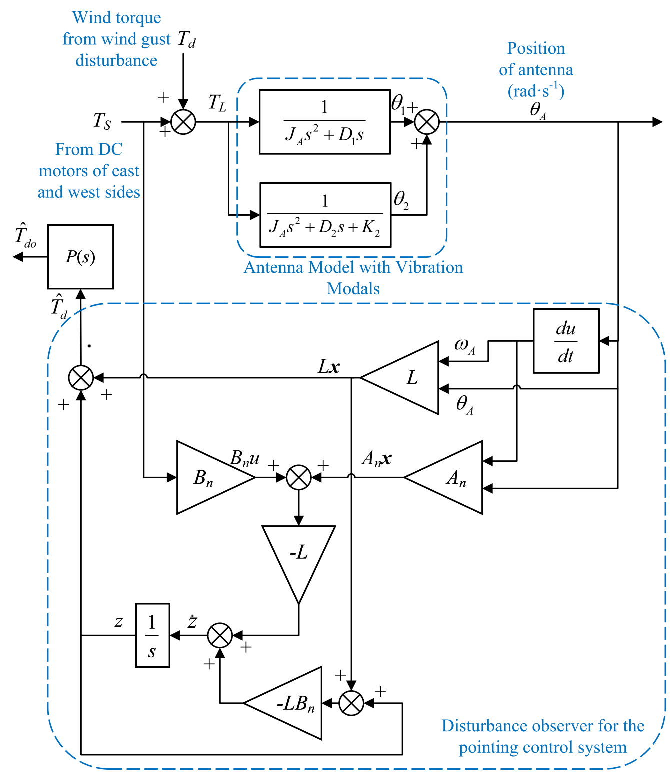

Figure 2. Diagram of the TD-DOB for LCT's pointing control system.

By combining Equations (19)–(24), the overall structure of the TD-DOB is designed as Figure 2 shows. The designed TD-DOB has the capability of estimating the composite external and internal disturbances since the output of the whole antenna model, rather than the output of the rigid body part of the antenna's model, is input to the TD-DOB.

3.2. LQR-Based Feedforward Controller for the DOB (LQR-DOB)

The output of the TD-DOB (i.e., $\widehat{T}_{do}$ in Equation (24)) is an estimation of the torque generated by the composite external and internal disturbances, which will be used to design a feedforward controller to compensate the real disturbance. A straight-forward idea is that if we can design a feedforward controller such that the output torque of the actuator (which includes the driver, the DC motors, and the reducer) can track $\widehat{T}_{do}$ accurately, then the torque generated by the disturbance will be compensated quite well.

According to LCT's pointing control system captured by Equation (15), we construct the state-space model that represents the relationship between the feedforward control signal (which is denoted by u_d) and the output torque of the

actuator (which is denoted by $\widetilde{T}_d$) as follows:

$$\begin{cases} \dot{\boldsymbol{x}}_d = A_g \boldsymbol{x}_d + B_g u_d \\ \widetilde{T}_d = C_g \boldsymbol{x}_d \end{cases} \tag{25}$$

[where $\boldsymbol{x}_d = \left[I^d_{\text{ARM}} \;\; \omega^d_{\text{DCM}} \;\; \theta^d_{\text{DCM}} \right]^T$ is the state vector, in which I^d_{ARM}, ω^d_{DCM} and θ^d_{DCM} are the armature current, the rotating speed, and the rotating angle of the DC motor respectively; and the matrices A_g, B_g, C_g are formulated as follows,

$$A_g = \begin{bmatrix} -\dfrac{R_{\text{DCM}}}{L_{\text{DCM}}} & -\dfrac{C_{\text{DCM}}}{L_{\text{DCM}}} & 0 \\ \dfrac{K_{\text{DCM}}}{J_{\text{DCM}}} & -\dfrac{\sigma_1}{J_{\text{DCM}}} & 0 \\ 0 & 1 & 0 \end{bmatrix}, \tag{26}$$

$$B_g = \begin{bmatrix} \dfrac{U_{\text{ARM}}/U_{COM}}{L_{\text{DCM}}} & 0 & 0 \end{bmatrix}, \tag{27}$$

$$C_g = \begin{bmatrix} 0 & 0 & \dfrac{K_{\text{RDC}}}{N} \end{bmatrix}. \tag{28}$$

In order to make $\widetilde{T}_d$ accurately track the output of the DOB, i.e., $\widehat{T}_{do}$, the estimation of the torque generated by the composite external and internal disturbances, a linear quadratic optimal tracking control problem is formulated as follows:

$$\min J = \frac{1}{2}\int_{t_0}^{\infty} [e^T(t)Qe(t) + u_d^T(t)Ru_d(t)] \tag{29}$$

$$\text{s.t.} \begin{cases} \dot{\boldsymbol{x}}_d(t) = A_g \boldsymbol{x}_d(t) + B_g u_d(t), \boldsymbol{x}_d(t_0) = \boldsymbol{x}_d^0 \\ \widetilde{T}_d(t) = C_g \boldsymbol{x}_d(t) \\ e(t) = \widehat{T}_{do}(t) - \widetilde{T}_d(t) \end{cases} \tag{30}$$

where $e(t)$ is the tracking error; $Q \in \mathbb{R}$ is the weight of the tracking error; $R \in \mathbb{R}$ is the weight of the feedforward control signal; and $\boldsymbol{x}_d^0$ is the initial state of the system.

According to the optimal control theory (Lewis et al. 2012), a linear quadratic regulator (LQR) can be designed to generate the approximate optimal control signal as follows

$$u_d(t) = -R^{-1}{B_g}^T \hat{P} \boldsymbol{x}_d(t) + R^{-1}{B_g}^T \hat{g} \tag{31}$$

where $\hat{P}$ is a positive definite matrix satisfying the following Algebraic Riccati Equation (ARE)

$$\hat{P}A_g + {A_g}^T\hat{P} - \hat{P}B_g R^{-1}{B_g}^T\hat{P} + {C_g}^T Q C_g = 0 \tag{32}$$

with

$$\hat{g} = [\hat{P}B_g R^{-1}{B_g}^T - {A_g}^T]^{-1}{C_g}^T Q \widehat{T}_{do} \tag{33}$$

Define $G = A_g - B_g R^{-1}{B_g}^T\hat{P}$, then the LQR-based feedforward controller for the DOB (LQR-DOB) can be finally designed as Figure 3 shows, where the estimated disturbance signal $\widehat{T}_{do}(t)$ is the input of the feedforward controller and $u_d(t)$ is the output of the feedforward controller. Note that the amplitude of the control signal $u_d(t)$ can be limited by adjusting the parameters Q and R.

3.3. DOB-Based Composite Position Controller with the Controller Switching Policy (DOB-CPC with CSP)

To reject the disturbance from LCT's pointing control system, the TD-DOB, LQR-based feedforward controller, and the feedback controller are combined as the DOB-based composite position controller (DOB-CPC) to replace the existing position controller (which is a proportional controller). Therefore, the control signal u_c generated by DOB-CPC consists of two parts: the feedback control signal u_b and the feedforward control signal u_d.

The first part is the feedback control signal u_b from the feedback controller (i.e., the existing proportional feedback controller or the H_∞ feedback controller proposed in our previous work (Chen & Wang 2022)), which calculates the control signal based on the position error of LCT's antenna. As LCT's pointing control system is captured by Equation (15), the H_∞ feedback controller can be obtained in many ways. Here the H_∞ loop-shaping technique (Glover & McFarlane 1989; Sefton & Glover 1990; Feyel 2013) is used to design the H_∞ feedback controller based on the model of LCT's pointing control system because it is easy to implement by designing the three loop-shaping weighting filters W_1, W_2, W_3 with the help of the MATLAB Robust Control Toolbox.[4] As Figure 4 shows, the error signal e, the control signal u, and the output signal y are input to the loop-shaping weighting filters W_1, W_2, W_3 (which can be set as the constant, the high-pass filter, or the low-pass filter) respectively to generate the measures of robustness z_1, z_2, z_3 (which are parts of the infinity norm of the closed-loop transfer function of the augmented model of LCT's pointing control system). Since the design of the H_∞ feedback controller aims to minimize the infinity norm of the closed loop transfer function of the pointing control system, the error signal e, the control signal u_c, and the output signal y can be adjusted by tuning W_1, W_2, W_3 respectively.

The second part is the feedforward control signal u_d from the LQR-based feedforward controller, which is obtained based on the estimated disturbance signal $\widehat{T}_{do}$ by using TD-DOB. Hence, the DOB-CPC not only makes full use of the characteristics of the feedback controller to quickly eliminate the position error, but also compensates the disturbance to further reduce the position fluctuation it generates.

Furthermore, as the step response plots shown in Figure 5, it should be noted that the H_∞ feedback controller and the LQR-based feedforward controller will bring negative impact on the rapidity of the transient process although they can greatly enhance the ability of disturbance rejection, especially for the circumstances under high-speed wind disturbances.

[4] https://www.mathworks.com/help/releases/R2022a/robust/ref/lti.hinfsyn.html

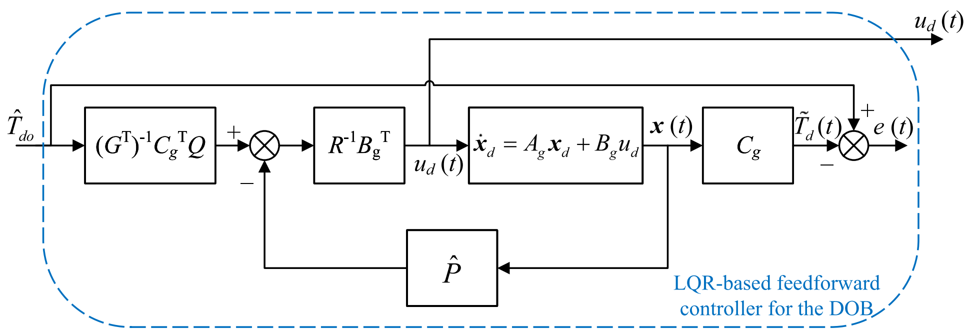

Figure 3. Diagram of the LQR-based feedforward controller for the DOB.

In specific, in the absence of wind disturbances (See Figure 5(a)), the transient process to the pointing control system with the H_∞ feedback controller is longer compared to the proportional (P) controller while the LQR-based feedforward controller (LQR-DOB) does not affect the pointing control system's transient performance. However, this situation changes significantly when facing large wind disturbances (See Figure 5(b)). In addition to the negative impact of the H_∞ feedback controller on the pointing control system's transient performance, the LQR-based feedforward controller (LQR-DOB) often generates overcompensation in the transient process, which leads to a significant delay in response. Thus, considering that the transient process under the existing proportional controller is the fastest (since the control signal is maintained at the maximum level), we propose a controller switching policy (CSP) for DOB-CPC. The key idea of the CSP is to activate the H_∞ feedback controller and the LQR-based feedforward controller only when the position of the antenna is within a certain range around the desired position (e.g., the orange area shown in Figure 6); otherwise, the existing proportional feedback controller works.

For the purpose of utilizing different controllers for the transient and steady-state stages respectively, then the CSP has the following form:

$$\begin{cases} u_c = u_p,\ |e_r| > \Delta h \\ u_c = k_b u_b + k_f u_d,\ |e_r| \leqslant \Delta h \end{cases} \tag{34}$$

where e_r is the position error of the antenna; $\Delta h \in [0, r]$ is the threshold of position error for activating H_∞ feedback control (which can also be replaced by the existing proportional feedback control, namely, keep using the existing proportional feedback control) and feedforward control; u_b is the feedback control signal; u_p is the control signal obtained by the existing proportional feedback controller; u_d is the control signal obtained by the LQR-based feedforward controller using the DOB-estimated disturbance signal; $k_b \in \mathbb{R}$ is the weight of the feedback control; and $k_f \in \mathbb{R}$ is the weight of the feedforward control. Here the equation that satisfies $|e_r| > \Delta h$ is for the transient process, and the equation that satisfies $|e_r| \leqslant \Delta h$ is for the steady-state process. By employing the CSP, the structure of DOB-CPC is depicted as the blue block in Figure 7.

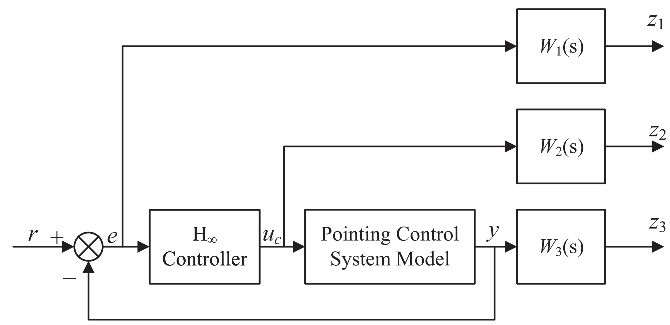

Figure 4. The diagram of closed-loop LCT's pointing control system with H_∞ feedback controller and loop-shaping weighting filters W_1, W_2, W_3: r is the reference input, e is the error signal, u_c is the control signal calculated by the H_∞ feedback controller, y is the system output signal, z_1, z_2, z_3 are the measures of robustness.

4. Simulation Experiments

4.1. Experiment Design

In this section, the experiment is divided into two parts:

(*1*) ***Mathematical Simulation Experiment***: MATLAB/Simulink is used to perform the simulation experiments for testing the performance of the proposed composite DOB-based position controller based on the mathematical model of LCT's pointing control system (whose antenna model includes a rigid body and the main structural modal). In this experiment, the performance of four types of position controllers (which are listed in Table 2) under the wind disturbance will be tested and compared.

(*2*) ***Collaborative Simulation Experiment***: Due to the unavailability of LCT during its relocation process, we developed a collaborative simulation testbed (Yao et al. 2023) to verify the performance of the proposed DOB-CPC (H_∞+LQR-DOB) by introducing a pre-constructed multibody dynamic model of the antenna.

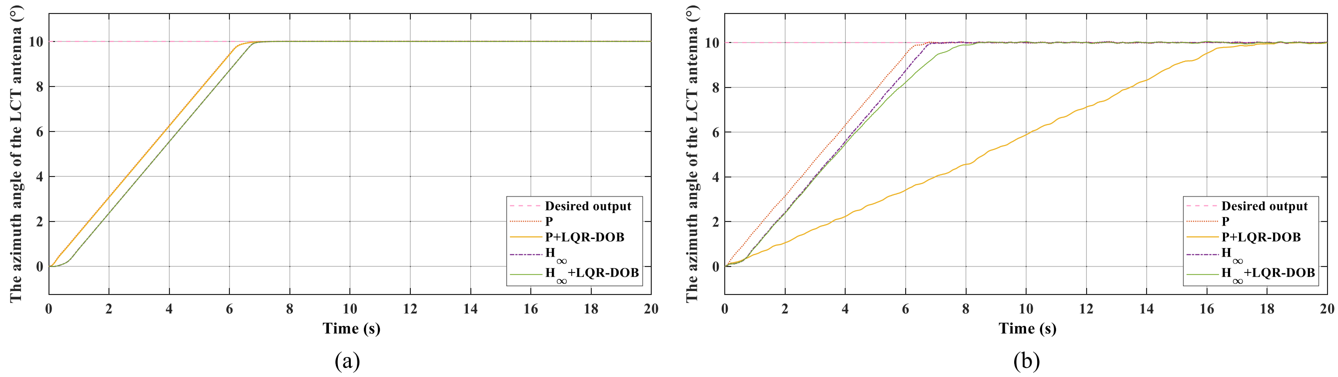

Figure 5. Step responses of the pointing control system using different controllers for two situations: (a) without wind disturbances; and (b) with 20 $\mathrm{m \cdot s^{-1}}$ wind disturbance.

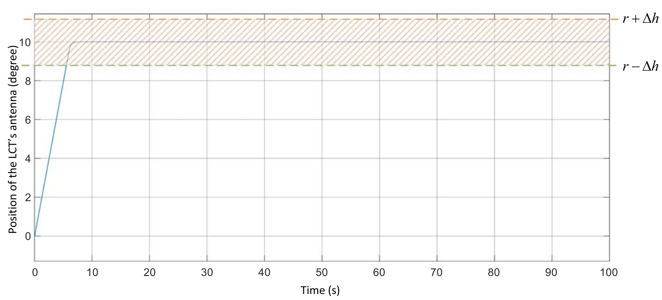

Figure 6. An example of the position of LCT's antenna. The range for activating the H_∞ feedback controller and the LQR-based feedforward controller is marked as the orange area.

As described in our previous research article (Yao et al. 2023), the Adams model is constructed based on the Ansys model of LCT. To be specified, as Figure 8 shows, we first constructed the mechanical structure of LCT using SpaceClaim (a 3D modeling tool within Ansys). The bodies of the mechanical structure have two categories, i.e., rigid bodies and flexible bodies. On one hand, rigid bodies can be well supported by Adams so that we can import them to Adams directly. On the other hand, flexible bodies are difficult to import to Adams directly since Adams is not good at building complex structural bodies. Therefore, we utilize Ansys to transform LCT's mechanical structure model to a finite elements model and proceed the modal analysis of LCT based on its finite elements model to obtain the modal neutral file of the flexible bodies. Finally, with the help of Adams, the rigid bodies (imported directly) and the flexible bodies (imported by the modal neural file) are integrated as a whole by applying the fixed joints to the contact surfaces between the rigid bodies and the flexible bodies.

With the help of the established Adams model, the simulation testbed is able to reflect the complex multimodal characteristics of the antenna in Simulink and its impacts on the dynamics of the entire pointing control system. (Without Adams, the complex multimodal characteristics of the antenna can only be analyzed statically in Ansys, which was not able to analyze the influence of these modals on the dynamics of the entire pointing control system).

Based on the existing model of the pointing control system, we replace the state-space formulation of the antenna by its multibody dynamics model, which was constructed using Adams (a multibody dynamics simulation software) by our team (Yao et al. 2023) to reduce the gap between the simulation model and the antenna in the real world. In addition, the multibody dynamics model of LCT's antenna has the same properties (i.e., material, dimensions, structures, density, and stiffness) as the antenna in the real world according to the on-site measurement and the Ansys model provided by our Chilean colleagues (See Acknowledgments) such that the accuracy of the multibody dynamics model of the antenna can be guaranteed. Then, with the collaborative simulation combining MATLAB/Simulink and Adams, we can further verify the proposed DOB-CPC (H_∞+LQR-DOB) on the collaborative simulation testbed (i.e., an integration of the mathematical model and the multibody dynamics model of the antenna, as shown in Figure 9). In this experiment, the proposed DOB-CPC (H_∞+LQR-DOB) will be tested on the mathematical model and the collaborative simulation testbed under different wind disturbances to observe whether it still works well in the situation close to the real world.

The wind disturbance consists of the wind gust (captured by the fluctuation of the wind speed, i.e., Δv_w) and the steady wind (captured by the average speed of the wind, i.e., v_w), in which the wind gust is the main factor leading to the rise of position error. Therefore, it is important to construct a good model for wind gust. To better describe wind gust, the Davenport filter is introduced, which is designed by following the instructions in Section 3 of Chen & Wang (2022). The power of the white noise (i.e., the source of the Davenport filter) and the average wind speed are adjustable for generating

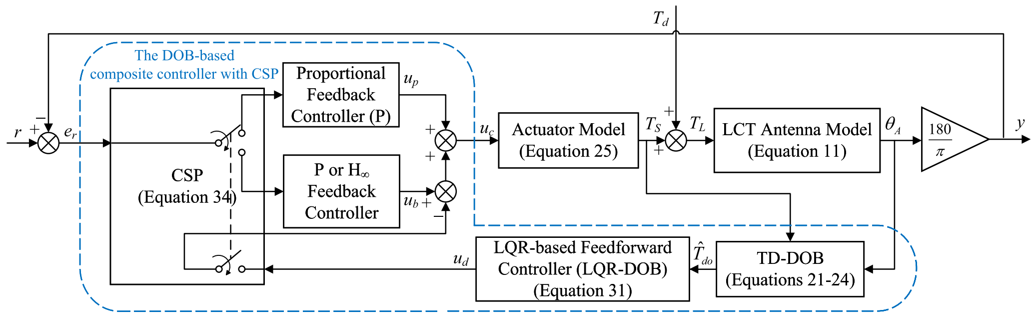

Figure 7. Diagram of LCT's pointing control system model when the DOB-based composite position controller (DOB-CPC) with CSP is implemented. "P" refers to the existing proportional feedback controller. "H_∞" refers to the H_∞ feedback controller.

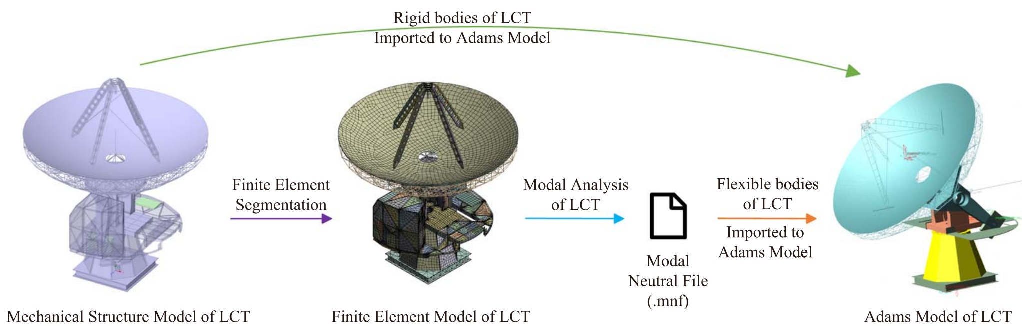

Figure 8. Diagram of the construction of the Adams model of LCT.

Table 2
Descriptions of Different Position Controllers to be Tested

Controller Type	Description
P	The existing proportional feedback controller
H_∞	The H_∞ feedback controller
DOB-CPC (P+LQR-DOB)	The DOB-based composite controller (DOB-CPC) shown in Figure 7 activates the existing proportional feedback controller and the LQR-based feedforward controller for the DOB (LQR-DOB) on the steady-state stage
DOB-CPC (H_∞+LQR-DOB)	The DOB-based composite controller (DOB-CPC) shown in Figure 7 that activating the H_∞ feedback controller and the LQR-based feedforward controller for the DOB (LQR-DOB) on the steady-state stage

wind disturbances of different average speeds and fluctuation amplitudes. According to the detail of the climate condition of the new site at Chajnantor Plateau, Chile, on one hand, the wind speed changes slowly during a day; on the other hand, the maximum amplitude of the wind speed fluctuation is 5 m s^{-1} (i.e., the wind speed fluctuates from 6 to 11 m s^{-1} during a day in winter) (ALMA 2010). Additionally, the average wind speed of the new site is 10 m s^{-1}, and the maximum wind speed of the new site is 30 m s^{-1} (ALMA 2010). Based on the above information, we have tested and compared the position control performance of four types of controllers under different average wind speeds and different wind gust fluctuations, where the average wind speed is set to three levels of 10, 15, and 20 m s^{-1}, and the amplitude of wind gust fluctuation is set to three levels of 2, 6, and 10 m s^{-1}. For convenience, the amplitude of wind gust fluctuations is measured by the following equation (see Figure 10):

$$A_{\Delta v_w} = |\Delta v_{w(\max)} - \Delta v_{w(\min)}| \tag{35}$$

where $A_{\Delta v_w}$ is the amplitude of wind gust fluctuations, $\Delta v_{w(\max)}$ is the maximum value of the wind gust fluctuations, and $\Delta v_{w(\min)}$ is the minimum value of the wind gust fluctuations. Then, the wind speed is converted to the equivalent wind disturbance torque (T_d) applied to the antenna's azimuth axis by multiplying a conversion factor (which is calculated based on the wind area of the antenna, the static air density, and the wind direction) according to the method described in (Chen & Wang 2022).

For the fairness of comparison, all controllers will be well tuned and then be tested in the same situation (i.e., the same target position (i.e., the azimuth angle) of the antenna, the same pointing control system model, and the same wind disturbance).

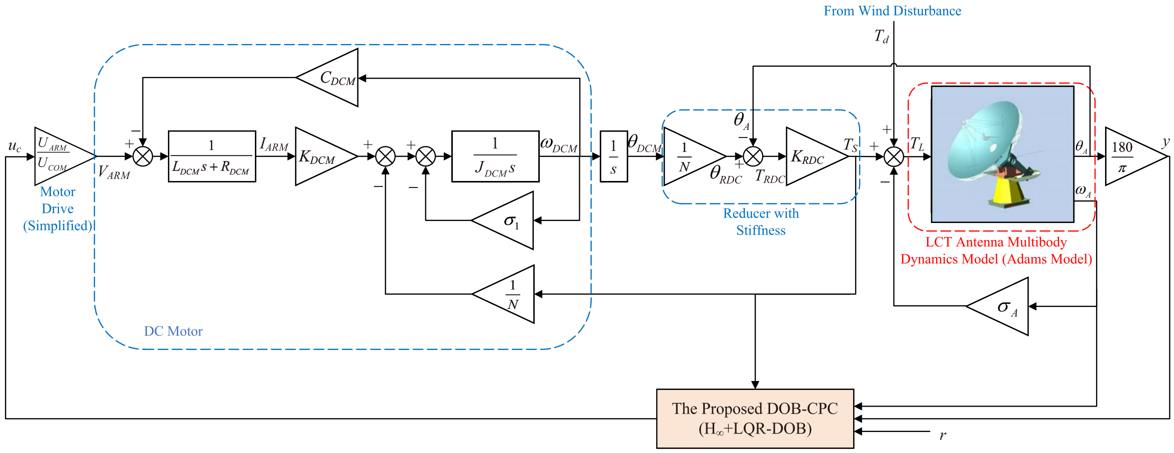

Figure 9. Collaborative simulation testbed for LCT's pointing control system (which has the Adams model of the antenna) when a DOB-based composite position controller (H_∞+LQR-DOB) is implemented. $\sigma_A = 1.7827 \times 10^6$ N · m · (rad · s^{-1})$^{-1}$ is the damping of LCT antenna.

We observe the output of LCT's pointing control system model (i.e., the position of the antenna) with different controllers (i.e., the existing proportional feedback controller, the H_∞ feedback controller, the DOB-CPC with existing proportional feedback controller, and DOB-CPC with H_∞ feedback controller) under the same wind disturbance, when the target position (i.e., the azimuth angle) is set as 10 deg.

The controllers are pre-configured as follows: First, the formulation and parameters of the existing proportional feedback controller are kept as given by the original technical report (Leighton 1977). Second, the H_∞ feedback controller is redesigned based on the state-space model of the pointing control system with vibration modals (see Equations (12)–(14)) by using the following loop-shaping weighting filters W_1, W_2, W_3: (1) W_1 is set as a low-pass filter such that the low-frequency gain (LFG) of W_1 is 5000 (i.e., 74 dB), the frequency corresponding to 0 dB magnitude of W_1 is 5 rad · s^{-1}, and the high-frequency gain (HFG) of W_1 is 0.1 (i.e., −20 dB); (2) W_2 is set as a constant, which is equivalent to 0.000 001; (3) W_3 is set as a high-pass filter such that the LFG of W_3 is 0.1 (i.e., −20 dB), the frequency corresponding to 0 dB magnitude is 6 rad · s^{-1}, and the HFG of W_3 is 5000 (i.e., 74 dB). The Bode diagram of W_1, W_3 is illustrated in Figure 11. Third, the parameters of the proportional feedback controller and the H_∞ feedback controller used in the DOB-CPC are the same as stated in the first two points, and the other undeclared parameters of DOB-CPC are tuned one by one for each case.

4.2. Simulation Results and Discussions

A. Mathematical Simulation Experiment

To carry out the mathematical simulation experiments, the parameters of the controllers are first well tuned, including: (1) the TD-DOB's parameters L, λ, which are the gain matrix of the TD-DOB and the parameter of the first-order low-pass filter $P(s)$ of the TD-DOB respectively (which can be found in Equations (21) and (23)); (2) the LQR-DOB's parameters Q, R, which are the weights of the tracking error and the feedforward control signal of the LQR-DOB respectively (which can be found in Equation (29)); (3) the CSP's parameters k_b, k_f, Δh, which are the weight of the feedback control signal u_b calculated by the feedback controller (proportional or H_∞), the weight of the feedforward control signal u_d calculated by the LQR-DOB, and the threshold of position error for activating H_∞ feedback control (or the existing proportional feedback control) and feedforward control respectively (which can be found in Equation (34)). Part of the parameters of the controllers are configured as Table 3 shows, and other unlisted parameters are set as follows: $Q = 15$, $k_b = 1$, $k_f = 1$ and $\Delta h = 0.1$ are adopted for all cases of simulation experiments.

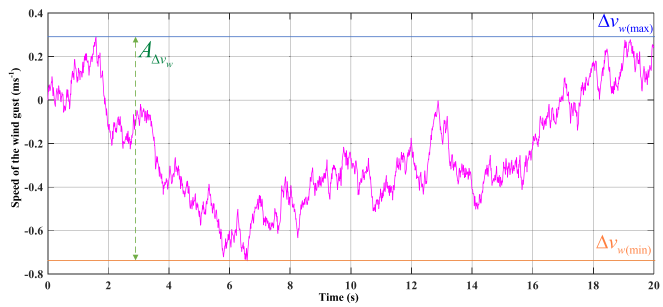

Figure 10. Diagram of the wind gust fluctuations.

Figures 12–14 present the position error of LCT's antenna using different controllers under different average wind speeds and the fluctuation amplitudes of 2, 6, and 10 m s^{-1} respectively. To further quantify and measure the disturbance rejection performance of the controllers, the root mean square (rms) of the position error is measured during the interval from

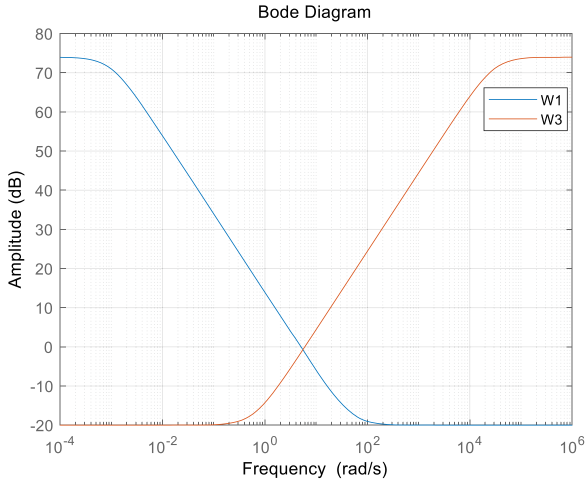

Figure 11. Bode diagram of loop-shaping filters W_1, W_3.

Table 3
Part of the Parameters of the Controllers for the Wind Disturbance of Different Average Wind Speeds and Fluctuation Amplitudes

Case Description	L	R	λ
$v_w = 10$ m s^{-1}, $A_{\Delta v_w} = 2$ m s^{-1}	$[100J_A \;\; 100J_A]$	0.3	0.001
$v_w = 10$ m s^{-1}, $A_{\Delta v_w} = 6$ m s^{-1}	$[100J_A \;\; 100J_A]$	0.3	0.001
$v_w = 10$ m s^{-1}, $A_{\Delta v_w} = 10$ m s^{-1}	$[100J_A \;\; 100J_A]$	0.3	0.001
$v_w = 15$ m s^{-1}, $A_{\Delta v_w} = 2$ m s^{-1}	$[100J_A \;\; 100J_A]$	0.3	0.001
$v_w = 15$ m s^{-1}, $A_{\Delta v_w} = 6$ m s^{-1}	$[100J_A \;\; 100J_A]$	0.3	0.001
$v_w = 15$ m s^{-1}, $A_{\Delta v_w} = 10$ m s^{-1}	$[100J_A \;\; 100J_A]$	0.3	0.001
$v_w = 20$ m s^{-1}, $A_{\Delta v_w} = 2$ m s^{-1}	$[100J_A \;\; 100J_A]$	0.3	0.001
$v_w = 20$ m s^{-1}, $A_{\Delta v_w} = 6$ m s^{-1}	$[100J_A \;\; 100J_A]$	0.3	0.003
$v_w = 20$ m s^{-1}, $A_{\Delta v_w} = 10$ m s^{-1}	$[100J_A \;\; 100J_A]$	0.3	0.003

the 10th s to the 20th s. Table 4 concludes the RMSs of the position error of LCT using different controllers under different average wind speeds and the fluctuation amplitudes of 2, 6, and 10 m s^{-1}.

From Figures 12–14, we can see that the transient performances of the pointing control system under the four controllers are almost the same because of the effectiveness of the CSP, i.e., the same proportional control is adopted before entering the steady state. Then, when the position error is within the range for activating H$_\infty$ control or feedforward control, the switching of controllers begins to show their strength on wind disturbance rejection. From Figures 12–14 and Table 4, we can see that the employment of the DOB-CPC controller (especially the H$_\infty$+LQR-DOB controller) can reduce the rms of the position error significantly. In addition, Figures 12–14 and Table 4 depict a clear trend that the position error increases with the rising of the wind average speed and the wind fluctuation amplitudes. However, even if under a high wind speed of 20 m s^{-1} and a large wind fluctuation of 10 m s^{-1}, the rms of position error can be reduced by more than 90%. For a lower wind speed of 10 m s^{-1} and a smaller wind fluctuation of 2 m s^{-1}, the rms of position error can be reduced by more than 92%.

On one hand, by comparing the position error under the existing proportional controller, the H$_\infty$ feedback controller, and the DOB-CPC (P+LQR-DOB), the position error of the LCT's pointing control system controlled by the H$_\infty$ feedback controller is first found much smaller than the one controlled by the existing proportional feedback controller. Moreover, once the DOB-CPC (P+LQR-DOB) is employed, the position error of the antenna is dramatically reduced compared to the one under the H$_\infty$ controller or the existing proportional feedback controller. Obviously, replacing the existing proportional controller by the H$_\infty$ controller, or combining the existing proportional controller with the LQR-DOB feedforward controller (i.e., the DOB-CPC controller), is helpful in reducing the position error of the antenna under the wind disturbance. In addition, the introduction of LQR-DOB feedforward controller contributes much more to eliminating the negative effect of wind disturbance on position control, compared with the contribution of the H$_\infty$ controller. This phenomenon can be explained by the principles of the H$_\infty$ controller and the LQR-DOB as follows: (1) The H$_\infty$ controller is capable of compressing the range of the position error to reduce the position error globally since it can improve the robustness of the system. (2) The LQR-DOB (which is integrated with the feedback controller as the DOB-CPC) provides an option of eliminating the negative effect of the external and internal disturbances precisely by estimating the disturbance signal using the DOB. Therefore, it achieves better performance compared to the H$_\infty$ controller.

On the other hand, by comparing the results of using the DOB-CPC (P+LQR-DOB) and the DOB-CPC (H$_\infty$+LQR-DOB), it can be found that the position error of the antenna is further reduced when the feedback controller of the DOB-CPC is changed from the existing proportional feedback controller to the H$_\infty$ feedback controller. A possible explanation for this phenomenon is that the combination of the H$_\infty$ controller and the LQR-DOB feedforward controller combines the strengths of both: rough disturbance rejection (compression of the range of position errors) with the H$_\infty$ feedback controller, and more refined disturbance rejection with the LQR-DOB feedforward controller.

The pointing accuracy of LCT is 3 arcsecond (3″) (rms), which requires that the rms of the position error of its pointing control must be less than 3″. However, the RMSs of the position errors in all cases using the existing proportional feedback controller exceed 3″, as shown in Table 4. After applying the proposed DOB-CPC (H$_\infty$+LQR-DOB), the RMSs of the position errors in all cases are greatly reduced by more than 90% accompanied by most cases achieving less than 3″. Nevertheless, the proposed DOB-CPC may have some

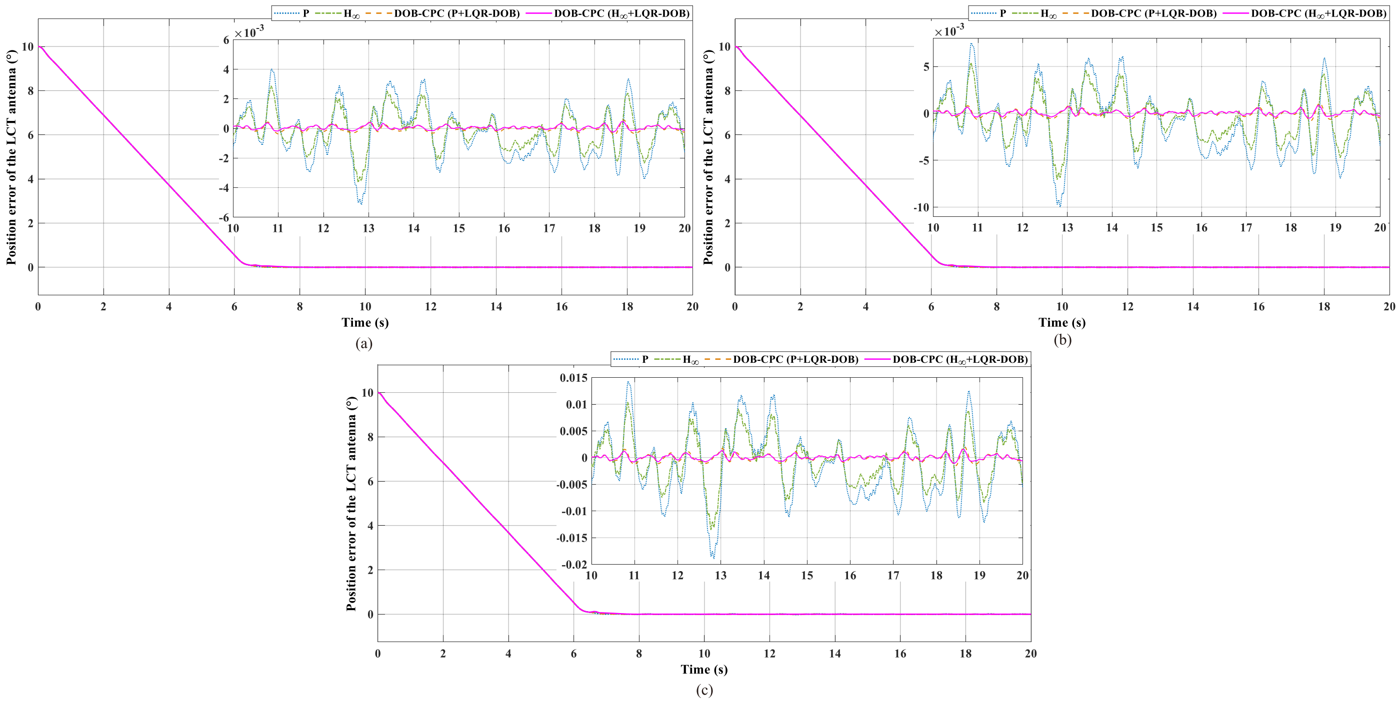

Figure 12. Position error of LCT's antenna using different controllers under different average wind speeds and the fluctuation amplitude of 2 m s^{-1}. (a) $v_w = 10$ m s^{-1}, $A_{\Delta v_w} = 2$ m s^{-1} (b) $v_w = 15$ m s^{-1}, $A_{\Delta v_w} = 2$ m s^{-1} (c) $v_w = 20$ m s^{-1}, $A_{\Delta v_w} = 2$ m s^{-1}.

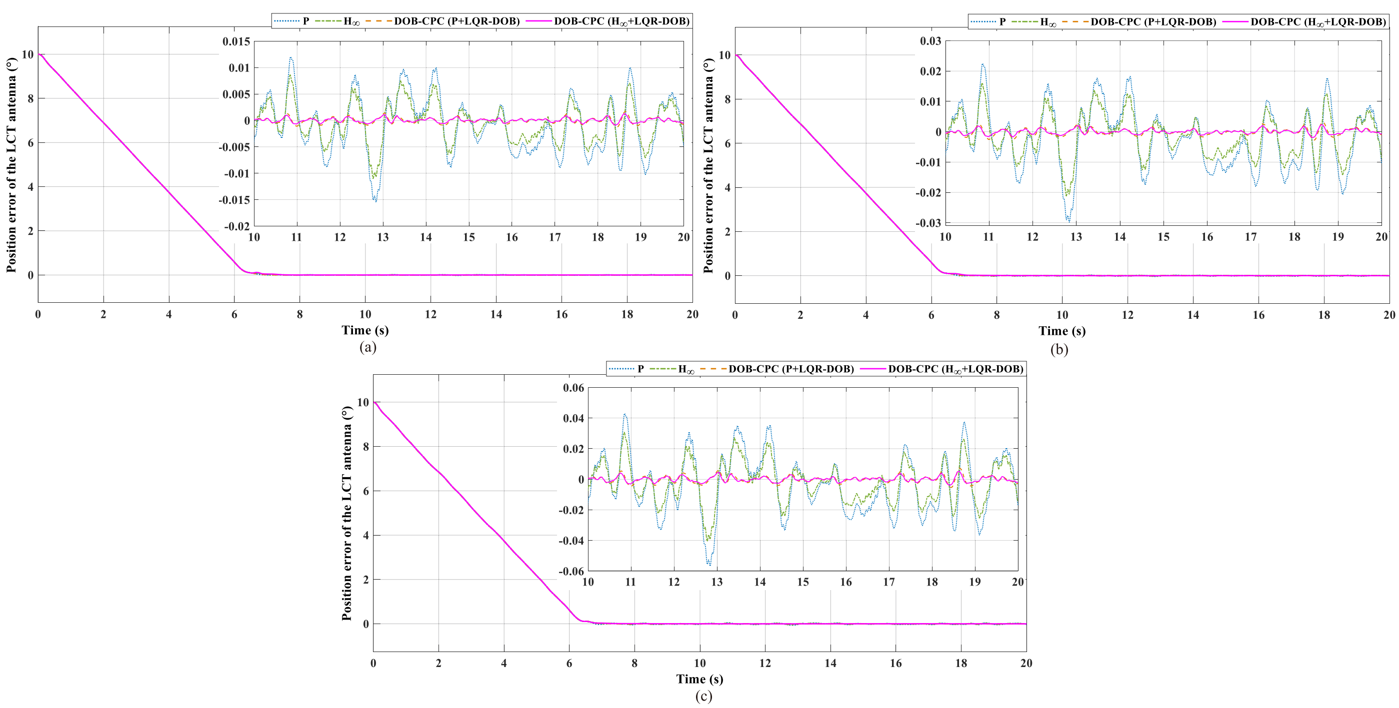

Figure 13. Position error of LCT's antenna using different controllers under different average wind speeds and the fluctuation amplitude of 6 m s^{-1}. (a) $v_w = 10$ m s^{-1}, $A_{\Delta v_w} = 6$ m s^{-1} (b) $v_w = 15$ m s^{-1}, $A_{\Delta v_w} = 6$ m s^{-1} (c) $v_w = 20$ m s^{-1}, $A_{\Delta v_w} = 6$ m s^{-1}.

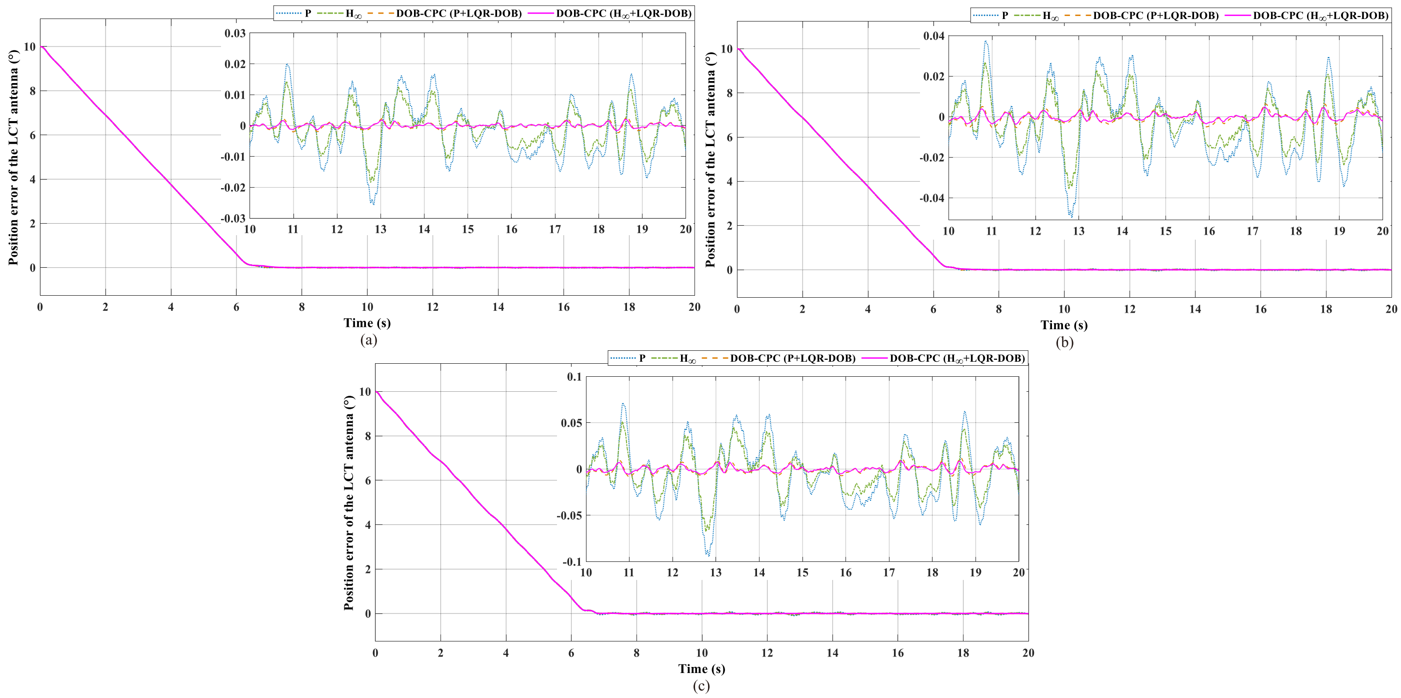

Figure 14. Position error of LCT's antenna using different controllers under different average wind speeds and the fluctuation amplitude of 10 m s^{-1}. (a) $v_w = 10$ m s^{-1}, $A_{\Delta v_w} = 10$ m s^{-1} (b) $v_w = 15$ m s^{-1}, $A_{\Delta v_w} = 10$ m s^{-1} (c) $v_w = 20$ m s^{-1}, $A_{\Delta v_w} = 10$ m s^{-1}.

Table 4
RMSs of the Position Errors of LCT's Antenna Using Different Controllers

Case Description	P	H$_\infty$	DOB-CPC (P+LQR-DOB)	DOB-CPC (H$_\infty$+LQR-DOB)	% of rms Decrease
$v_w = 10$ ms^{-1}, $A_{\Delta v_w} = 2$ ms^{-1}	4.″626	3.″173	0.″461	**0.″366**	92.09%
$v_w = 10$ ms^{-1}, $A_{\Delta v_w} = 6$ ms^{-1}	13.″860	9.″534	1.″377	**1.″001**	92.78%
$v_w = 10$ ms^{-1}, $A_{\Delta v_w} = 10$ ms^{-1}	23.″110	15.″900	2.″348	**1.″680**	92.73%
$v_w = 15$ ms^{-1}, $A_{\Delta v_w} = 2$ ms^{-1}	8.″946	6.″108	0.″872	**0.″648**	92.76%
$v_w = 15$ ms^{-1}, $A_{\Delta v_w} = 6$ ms^{-1}	26.″770	18.″320	2.″800	**1.″987**	92.58%
$v_w = 15$ ms^{-1}, $A_{\Delta v_w} = 10$ ms^{-1}	44.″800	30.″670	6.″466	**4.″479**	90.00%
$v_w = 20$ ms^{-1}, $A_{\Delta v_w} = 2$ ms^{-1}	16.″850	11.″590	1.″673	**1.″214**	92.80%
$v_w = 20$ ms^{-1}, $A_{\Delta v_w} = 6$ ms^{-1}	50.″540	34.″800	5.″856	**4.″230**	91.63%
$v_w = 20$ ms^{-1}, $A_{\Delta v_w} = 10$ ms^{-1}	84.″210	58.″000	10.″920	**7.″856**	90.67%

Note. Under Different Wind Disturbances of Different Average Speeds and Fluctuation Amplitudes.

limitations on its performance for some extreme cases, which are (1) the wind disturbances with an average speed of 15 m s^{-1} and the fluctuation of 10 m s^{-1} and (2) the wind disturbances with the average speed of 20 m s^{-1} and the fluctuation above 6 m s^{-1}. The above results provide some instructions of applying the DOB-CPC properly. If a high pointing accuracy (e.g., 3″) is required during LCT's operation, employing the DOB-CPC can achieve this aim when the wind disturbance is not very large (e.g., a relatively low average speed of 10 m s^{-1}, or a relatively small fluctuation of 2 m s^{-1}). If the wind disturbance is relatively large (i.e., an average speed of 20 m s^{-1}, or a relative medium fluctuation of 6 m s^{-1}) but the requirement on the pointing accuracy is not very high (e.g., above 3″ but below 10″), the DOB-CPC still works well.

In general, by carrying out the above tests, we find that the proposed DOB-CPC can help LCT's pointing control system to deal with different types of wind disturbances and achieve significant performance improvement compared to the single feedback controller (i.e., the proportional controller or the H$_\infty$ controller). Thus, the accurate estimation of disturbance signals by TD-DOB and the accurate generation of the feedforward control signal by LQR together eliminate the negative effect of

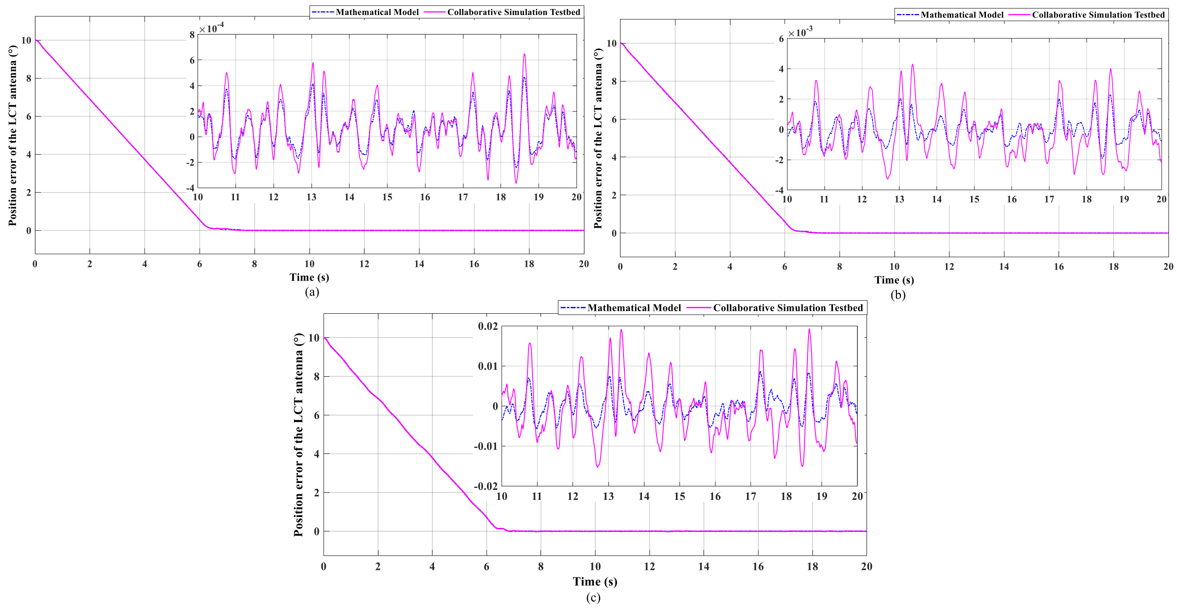

Figure 15. Position error of LCT antenna using the proposed DOB-CPC (H_∞+LQR-DOB) on both the mathematical model and the collaborative simulation testbed under different wind disturbances (a) $v_w = 10$ m s^{-1}, $A_{\Delta v_w} = 2$ m s^{-1} (b) $v_w = 15$ m s^{-1}, $A_{\Delta v_w} = 6$ m s^{-1} (c) $v_w = 20$ m s^{-1}, $A_{\Delta v_w} = 10$ m s^{-1}.

the external and internal disturbances caused by wind load and structural flexibility of the antenna.

B. Collaborative Simulation Experiment

By integrating LCT's pointing control system model and the multibody dynamics model of LCT's antenna, we can conduct the collaborative simulation experiment to further verify the performance of the proposed DOB-CPC (H_∞+LQR-DOB) in the situation closer to reality. This experiment is conducted under three typical wind disturbances, which are (a) $v_w = 10$ m s^{-1}, $A_{\Delta v_w} = 2$ m s^{-1} (b) $v_w = 15$ m s^{-1}, $A_{\Delta v_w} = 6$ m s^{-1} (c) $v_w = 20$ m s^{-1}, $A_{\Delta v_w} = 10$ m s^{-1}. Considering that the dynamics of the antenna in the state-space formulation is different from the dynamics of the antenna in the Adams model (which contains more vibration modals and nonlinear characteristics that are not captured by the state-space formulation), the former well-tuned parameters of the controllers need to be adjusted for adapting the Adams model in the collaborative simulation testbed: (1) change λ from 0.001 to 0.006 for the case of $v_w = 10$ m s^{-1}, $A_{\Delta v_w} = 2$ m s^{-1}; (2) change λ from $v_w = 15$ m s^{-1}, $A_{\Delta v_w} = 6$ m s^{-1}; (3) change λ from 0.003 to 0.02 for the case of $v_w = 20$ m s^{-1}, $A_{\Delta v_w}$ =10 m s^{-1}.

Figure 15 shows the position error of LCT's antenna under the DOB-CPC (H_∞+LQR-DOB) for both the mathematical model (i.e., the state space model) and the collaborative simulation testbed (i.e., the state space model integrated with the Adams model of antenna) under different wind disturbances, and the RMSs of the position errors are also calculated and shown in Table 5. Figure 15 and Table 5 indicate that the performance of the proposed DOB-CPC (H_∞+LQR-DOB) on the collaborative simulation testbed is almost the same as the one on the mathematical model under the most often-seen wind disturbance (i.e., $v_w = 10$ m s^{-1}, $A_{\Delta v_w} = 2$ m s^{-1}). However, for stronger wind disturbances, the proposed DOB-CPC (H_∞+LQR-DOB) performs relatively worse on the collaborative simulation testbed than on the mathematical model: the position error increases from 1.″9860 to 4.″0290 for the case of $v_w = 15$ m s^{-1}, $A_{\Delta v_w} = 6$ m s^{-1}, and from 7.″8560 to 18.″3300 for the case of $v_w = 20$ m s^{-1}, $A_{\Delta v_w} = 10$ m s^{-1}. Despite of the degradation of performance in these two cases, the position error of 4.″0290 is still acceptable under the average wind speed of 15 m s^{-1} and the fluctuation of 6 m s^{-1}. Actually, at LCT's new site on Chajnantor Plateau in Chile, the first two cases of wind load are much more common than the third case. Therefore, the result of this experiment verifies the feasibility of applying the proposed DOB-CPC (H_∞+LQR-DOB) on LCT's pointing control system after it is relocated and refurbished in Chile.

5. Conclusions

In this paper, a disturbance observer-based composite position controller (DOB-CPC) for LCT's pointing control system is proposed to realize a better performance of disturbance rejection under high wind loads. Since the key issue for implementing disturbance observer-based control is to generate proper compensation control signal when the types of the control signal and the disturbance signal are different, an optimal control model with a linear quadratic regulator (i.e., LQR-DOB) is constructed to precisely generate the

Table 5
RMSs of the Position Errors Of LCT Antenna Using the Proposed DOB-CPC (H_∞+LQR-DOB) on Different Models Under Different Wind Disturbances (Time Duration: 10–20 s)

Average wind speeds and fluctuation amplitudes	Mathematical model	Collaborative simulation testbed
$v_w = 10$ m s^{-1}, $A_{\Delta v_w} = 2$ m s^{-1}	0.″3658	0.″5081
$v_w = 15$ m s^{-1}, $A_{\Delta v_w} = 6$ m s^{-1}	1.″9860	4.″0290
$v_w = 20$ m s^{-1}, $A_{\Delta v_w} = 10$ m s^{-1}	7.″8560	18.″3300

compensation control signal, which can make the actuator output proper physical quantity relatively close to the estimated disturbance and consequently compensate the disturbance as much as possible. Finally, to maintain the rapidity of the transient process and acquire the disturbance rejection performance provided by the LQR-DOB feedforward controller and the H_∞ feedback controller at the same time, a controller switching policy is designed to integrate the LQR-DOB feedforward controller, the H_∞ feedback controller, and the existing proportional controller as an observer-based composite position controller (DOB-CPC).

To further verify the performance of the proposed DOB-CPC (H_∞+LQR-DOB), we conduct simulation experiments, which includes mathematical simulation experiment and collaborative simulation experiment, for LCT's pointing control system. The results of the mathematical simulation experiment indicate that the proposed DOB-CPC (H_∞+LQR-DOB) performs much better than other controllers for all types of wind disturbances. Meanwhile, the results of numerical experiments on the collaborative simulation testbed (i.e., the collaborative simulation experiment), which integrates the multibody dynamics model of antenna constructed by Adams, further ensures that proposed DOB-CPC (H_∞+LQR-DOB) is applicable in practice.

Once the relocation and refurbishment of LCT is completed in 2024, the proposed DOB-CPC (H_∞+LQR-DOB) will be verified physically during the astronomical observation to further evaluate its capability of achieving high precision pointing accuracy under large wind load. Based on this, our future work will focus on enhancing the integration between the proposed pointing control method (i.e., DOB-CPC) and the pointing correction technique to further improve the pointing accuracy of LCT.

Acknowledgments

We would like to thank Nicolás Lastra Inzunza, Brian Andler Prendergast, and David Arroyo Reyes, from the University of Concepción, Chile, for providing us with the Ansys model of LCT as a basis for our modal analysis. We also thank Mr. Yiwei Yao, from Southeast University, China, for his efforts on vibration modal analysis of LCT.

ORCID iDs

Weirui Chen https://orcid.org/0000-0003-2603-6338
Zheng Wang https://orcid.org/0000-0001-9051-6569

References

ALMA 2010, Climate Conditions at the Chajnantor Site, https://almascience.nrao.edu/about-alma/weather/overview
Burns, M. K. 1995, Proc. SPIE, 2479, 218
Caltech, CAS, & UdeC 2016, Conceptual Design Report for Leighton Chajnantor Telescope, Report, California Institute of Technology
Chen, W., & Wang, Z. 2022, Proc. SPIE, 12187, 121870T
Chen, W., Wang, Z., & Zhou, X. 2022, PASP, 134, 105002
Chen, W.-H., Yang, J., Guo, L., & Li, S. 2016, ITIE, 63, 1083
Choi, Y., Yang, K., Chung, W. K., Kim, H. R., & Suh, I. H. 2003, ITAC, 48, 315
Dai, C., Guo, T., Yang, J., & Li, S. 2021, ITIE, 68, 767
Deng, Y., Xia, P., Li, H., & Wang, X. 2018, Meas, 129, 245
Feng, H., & Guo, B.-Z. 2017, ITAC, 62, 3774
Feyel, P. 2013, Two Degrees-of-Freedom Controllers, Loop-shaping Robust Control (London: Wiley-ISTE), 135
Gawronski, W. 2001, IAPM, 43, 52
Gawronski, W. 2008, Analytical Models, Modeling and Control of Antennas and Telescopes (Boston, MA: Springer), 11
Gawronski, W., & Parvin, B. 1995, Simulations of the GBT Antenna with LQG Controller, Report 136, NRAO
Gawronski, W., Racho, C., & Mellstrom, J. 1994, IFAC Proceedings Volumes, 27, 393
Gawronski, W., & Souccar, K. 2005, IAPM, 47, 41
Glover, K., & McFarlane, D. 1989, ITAC, 34, 821
Guo, B.-Z., Wu, Z.-H., & Zhou, H.-C. 2016, ITAC, 61, 1613
Huang, Z., & Chen, M. 2022, ITCSII, 69, 3545
Leighton, R. B. 1977, A 10-Meter Telescope for Millimeter and Sub-Millimeter Astronomy, Report AST 73-04908, California Inst. Technology
Lewis, F. L., Vrabie, D. L., & Syrmos, V. L. 2012, The Tracking Problem and Other LQR Extensions, Optimal Control (San Francisco, CA: John Wiley & Sons, Ltd), 177
Li, P., Bao, H., Wei, S., & Xu, Q. 2017, SSPMA, 47, 059510
Li, S., Yang, J., Chen, W.-H., & Chen, X. 2016, Disturbance Observer-Based Control: Methods and Applications (Boca Raton, FL: CRC Press), 14
Li, X., Zhou, W., Luo, J., Qian, J., & Ma, W. 2019, in Chinese Control Conference (CCC) (Guangzhou, China: CCC), 3145
Maneri, E., & Gawronski, W. 2000, ISAT, 39, 243
Pan, H., Sun, W., Gao, H., & Jing, X. 2016, ITASE, 13, 868
Qian, Y., & Fang, Y. 2019, ITASE, 16, 1125
Qiu, D., Sun, M., Wang, Z., Wang, Y., & Chen, Z. 2014, ITCST, 22, 1983
Ranka, T., Garcia-Sanz, M., & Ford, J. M. 2015, in ASME 2015 Dynamic Systems and Control Conference *(Columbus, Ohio, USA)*
Ranka, T. M., Garcia-Sanz, M., Symmes, A. H., Ford, J. M., & Weadon, T. L. 2016, JATIS, 2, 014001
Ravensbergen, M. 1994, Proc. SPIE, 2199, 997
Sadhu, S., & Ghoshal, T. K. 2011, ITCST, 19, 449
Schipani, P., Gonzalez, M., Perrotta, F., et al. 2020, Proc. SPIE, 11445, 1144552
Sefton, J., & Glover, K. 1990, Systems & Control Letters, 14, 295
Shang, D., Li, X., Yin, M., & Li, F. 2022, AEJ, 61, 4741
Tripathi, V. K., Yogi, S. C., Kamath, A. K., et al. 2022, ISysJ, 16, 1649
Vial, J., Arroyo, D., Canales, C., et al. 2020, Proc. SPIE, 11445, 114453C
Wu, X., Xu, K., Lei, M., & He, X. 2020, ITASE, 17, 2182
Yang, J., Chen, W.-H., Li, S., Guo, L., & Yan, Y. 2017, ITIE, 64, 3273
Yao, Y.-W., Chen, W.-R., & Wang, Z. 2023, RAA, 23, 045013